IJMMM International Journal of Minerals, Metallurgy and Materials 矿物冶金与材料学报（英文版）

Adsorption properties of V(IV) on resin-activated carbon composite electrodes in capacitive deionization

Xiao-man Tian, Shen-xu Bao, and Yi-min Zhang

Cite this article as:
Xiao-man Tian, Shen-xu Bao, and Yi-min Zhang, Adsorption properties of V(IV) on resin-activated carbon composite electrodes in capacitive deionization, *Int. J. Miner. Metall. Mater.*, 28(2021), No. 11, pp. 1777-1787. https://doi.org/10.1007/s12613-020-2100-6

View the article online at SpringerLink or IJMMM Webpage.

International Journal of Minerals, Metallurgy and Materials
Volume 28, Number 11, November 2021, Page 1777
https://doi.org/10.1007/s12613-020-2100-6

Adsorption properties of V(IV) on resin-activated carbon composite electrodes in capacitive deionization

Xiao-man Tian[1)], *Shen-xu Bao*[1,2)], *and Yi-min Zhang*[1,2,3)]

1) School of Resources and Environmental Engineering, Wuhan University of Technology, Wuhan 430070, China
2) Hubei Key Laboratory of Mineral Resources Processing and Environment, Wuhan University of Technology, Wuhan 430070, China
3) Hubei Collaborative Innovation Center for High Efficient Utilization of Vanadium Resources, Hubei Provincial Engineering Technology Research Center of High Efficient Cleaning Utilization for Shale Vanadium Resource, Wuhan University of Science and Technology, Wuhan 430081, China
(Received: 6 April 2020; revised: 13 May 2020; accepted: 15 May 2020)

Abstract: Composite electrodes prepared by cation exchange resins and activated carbon (AC) were used to adsorb V(IV) in capacitive deionization (CDI). The electrode made of middle resin size (D860/AC M) had the largest specific surface area and mesoporous content than two other composite electrodes. Electrochemical analysis showed that D860/AC M presents higher specific capacitance and electrical double layer capacitor than the others, and significantly lower internal diffusion impedance. Thus, D860/AC M exhibits the highest adsorption capacity and rate of V(IV) among three electrodes. The intra-particle diffusion model fits well in the initial adsorption stage, while the liquid film diffusion model is more suitable for fitting at the later stage. The pseudo-second-order kinetic model is suited for the entire adsorption process. The adsorption of V(IV) on the composite electrode follows that of the Freundlich isotherm. Thermodynamic analysis indicates that the adsorption of V(IV) is an exothermic process with entropy reduction, and the electric field force plays a dominant role in the CDI process. This work aims to improve our understanding of the ion adsorption behaviors and mechanisms on the composite electrodes in CDI.

Keywords: capacitive deionization; composite electrode; vanadium; electrochemical behavior; kinetics

1. Introduction

As a rare metal, vanadium is commonly used in the iron-steel, chemical, aerospace, new energy, and alloy industries [1−2]. Leaching is the primary method to extract vanadium from the vanadium-bearing resources [3−4], such as fly ash [5] and stone coal [6]. Therefore, enriching and separating vanadium from leachate are indispensable tasks in the extraction industry [7]. At present, the purification and enrichment of vanadium from leaching solutions are mainly conducted by solvent extraction (SX) and ion exchange (IX) [8], but these two techniques have limitations. For example, the IX process is time-consuming and the IX resin is less adaptable. The SX process is less efficient, and the loss of the extraction agent is harmful to the environment [9−10]. Thus, an emerging ion separation and purification technique, capacitive deionization (CDI), has been attracting the attention of many researchers and was tried to be introduced into the field of hydrometallurgy.

CDI uses the principles of ionic adsorption on electrode through electrostatic force [11]. When a low direct electrical field is established, the charged ions are constrained toward the oppositely charged electrodes and form an electric double layer (EDL) on the surface of the electrodes [12−13]. Thus, CDI is an economical, efficient, and environmentally friendly separation technique. CDI originally is just proposed for desalination of seawater or brackish water because it is characterized by poor selective adsorption for ions [14]. However, some studies have demonstrated that the combination of capacitor deionization and IX can achieve the separation and enrichment of certain ions by using the composite electrodes [15−17]. IX resins pose diverse functional groups and present strong selective adsorption capacity for specific ions. The composite electrode prepared by using the IX resin and carbon material can improve the adsorption performance of the electrode to the target ions [18−19]. Our group prepared resin/activated carbon (AC) composite electrodes by using AC and different IX resins, which have been successfully used to remove vanadium from a complex leaching solution [20]. However, studies have only focused on the pre-

Corresponding author: Shen-xu Bao E-mail: sxbao@whut.edu.cn

paration of the composite electrodes and ion adsorption properties on the electrodes. Few studies have systematically investigated the effect of resin particle size on the properties of the composite electrodes as well as the adsorption kinetics and thermodynamics of ions. CDI is a nonlinear dynamical process, and the ion adsorption on electrodes involves complex ion motion and adsorption mechanisms. An understanding of the properties and adsorption characteristics of electrodes is essential to enhance the performance of CDI on the separation of ions.

As mentioned, our previous study showed that D860, an amino phosphoric acid chelating cation exchange resin, has strong affinity to tetravalence vanadium (V(IV)), and the composite electrode made of D860 and AC also presents high adsorption capacity and strong selectivity for V(IV). In the present study, D860 with different sizes was selected to prepare composite electrode with AC and used to adsorb V(IV) from aqueous solution. The physical and chemical properties of the composite electrode were investigated by Brunauer−Emmett−Teller (BET), electrochemical and Fourier transform infrared (FT-IR) spectroscopy analysis. The adsorption kinetics, isotherms, and thermodynamics were also evaluated to investigate the ion adsorption characteristics.

2. Experimental

2.1. Materials

D860 cation exchange resin with high affinity for V(IV), which was purchased from Zhengguang Industrial Co. Ltd., China, and AC provided by Durban Activated Carbon Co. Ltd., China, were utilized to prepare D860/AC composite electrode in this study. Vanadyl sulfate ($VOSO_4$) with analytical reagent (A.R.) grade was used to prepare V(IV) feed solution (VO^{2+}). N-dimethylacetamide (DMAC) and polyvinylidene fluoride (PVDF) with A.R. grade were obtained from Sinopharm Chemical Reagent Co. Ltd., China and Sigma Aldrich Chemical Reagent Co. Ltd., China, respectively. High-purity graphite flake came from Haimen Shuguang Carbon Industry Co. Ltd., China.

2.2. Preparation

2.2.1. Materials pretreatment

AC was ground to pass through a 38 μm sieve. D860 resin was soaked in 5wt% NaOH solution, followed by washing until the supernatant was nearly neutral. Thereafter, the resin was soaked in 5vol% HCl solution for 24 h. The resin was then washed with deionized water until the supernatant was nearly neutral. After the cleaning procedure, the resin was filtrated and dried to the constant weight at 60°C. Finally, the resin was ground in the vibration mill for 20 min and sieved by the shaking screen to obtain the products with a particle diameter of 37−45, 53−63, and 125−150 μm, respectively. A suitable amount of $VOSO_4$ was dissolved in deionized water to prepare the V(IV) feed solution.

2.2.2. Preparation of composite electrodes

The preparation schematic of the composite electrode is shown in Fig. 1. To fabricate composite electrodes, we first prepared a composite material slurry by mixing 0.5 g AC, 0.5 g D860 resin, and 0.1 g PVDF in 4.0 mL DMAC, which was stirred for 4 h at 25°C to ensure thorough dispersion. DMAC was used as a solvent to fully mix the D860 and AC, and PVDF was used to bind the high-purity graphite flake with the composite material. Then, the slurry was painted on the high-purity graphite flakes with dimensions of 50 mm (width) × 100 mm (length) × 1 mm (thickness). The composite electrodes were prepared by drying for 4 h at 60°C in a vacuum oven to ensure that DMAC was completely volatilized. The dry weight of the composite material on each graphite was approximately 1.2−1.6 g. The composite electrodes using resins with particle size of 37−45, 53−63, and 125−150 μm were labeled as D860/AC S, D860/AC M, and D860/AC C, respectively.

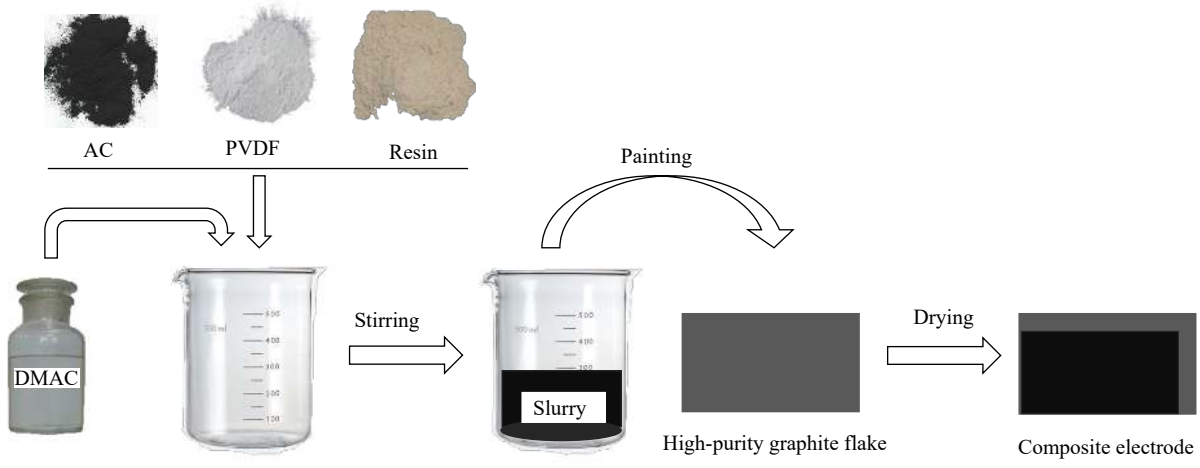

Fig. 1. Schematic of preparation of composite electrode.

2.3. Capacitive deionization experiments

The CDI cell, peristaltic pump, and constant voltage direct-current (DC) supply were used to form an electric adsorption device [21]. The DC supply and peristaltic pump were respectively provided by Zhaoxin Electronic Equipment Co. Ltd., China, and Natong Peristaltic Pump Manufacture Co. Ltd., China. The CDI cell used in this study was assembled using parallel-aligned electrodes (five composite electrodes and four graphite flakes), which were placed in a polymethyl methacrylate tank. In the experiments, the high-purity graphite flakes without coating were used as anode and the D860/AC composite electrodes were used as cathode. The flow rate was sustained at 30 mL/min, and the space between the two electrodes was 3 mm. Each pair of parallel electrodes was supplied a voltage of 1.0 V. 200 mL feed solution with initial pH of 2.0 was pumped into the CDI cell by peristaltic pump for circular treatment. The concentration of vanadium in the solution was measured through the ammonium ferrous sulfate titration method (GB/T8704.5—2007) and the adsorption capacity of the composite electrodes for vanadium was defined as:

$$q_t = \frac{C_0 \times V_0 - C_t \times V_t}{m} \times 100\% \quad (1)$$

where q_t is the adsorption capacity of the composite electrodes at time t (mg/g), C_t and V_t are the ion concentration in the aqueous solution (mg/L) and the solution volume (L) at time t, respectively, C_0 and V_0 are the initial ion concentration in the aqueous solution (mg/L) and the initial solution volume (L), respectively, and m is the mass of D860/AC composite material on the graphite flake (g).

For kinetics study, 200 mL feed solution with initial vanadium concentration of 1000 mg/L at 25°C was treated by CDI and 1 mL solution was sampled at predetermined intervals ranging from 0 to 380 min to determine vanadium concentration. Adsorption isotherm experiments were conducted at 25°C with different initial vanadium concentrations from 820 to 1000 mg/L. A thermodynamic adsorption study was conducted at the temperatures of 25, 30, 35 and 40°C, using D860/AC M with initial vanadium concentration of 1000 mg/L. The adsorption time was fixed at 380 min for the adsorption isotherm and thermodynamic investigation.

2.4. Characterization of composite electrodes

The composite electrode material was scraped from the graphite flake with a blade for properties analysis. The porosity of the electrode material was observed from the isotherm adsorption branch with the Barrett−Joyner−Halenda (BJH) method [22]. The specific surface area (S_{BET}) of the material was determined through the BET method using ASAP 2020M surface and pore size analyzer (Micromeritics Instruments, US).

The structural variations of the electrode material before and after adsorption were examined using a Nexus spectrometer (Thermo Nicolet Co. Ltd., US). The FT-IR spectra of the samples were noted in the range of 4000−450 cm^{-1} at room temperature.

Cyclic voltammetry (CV) and electrochemical impedance spectroscopy (EIS) were conducted by an electrochemical workstation (AMETEK, VersaSTAT4, US). These measurements were performed using a three-electrode cell consisting of a counter electrode (platinum wire), a working electrode (D860/AC electrode), and a reference electrode (Ag/AgCl) at 25°C. The CV measurements were conducted in the potential range of −0.3 to 0.9 V at a specific scan rate of 20 mV/s, and the cyclic scanning was performed 3 times. EIS measurements were conducted using alternating current perturbation amplitude of 5 mV around the equilibrium potential (0 V). The data were collected in the frequency range from 105 to 0.1 Hz.

2.5. Adsorption kinetic models

The pseudo-first-order kinetic model, which is commonly used in liquid-phase adsorption, assumes that the adsorption rate is controlled by physisorption [23]. The pseudo-second-order kinetic model assumes that the adsorption process is dominated by the chemical reaction [24], which involves electron transfer or sharing between the adsorbate and the adsorbent [25]. The Elovich kinetic equation is an empirical formula derived from the chemistry theory of the gas−solid interface. It is appropriate for most adsorption processes and is mainly used to describe the chemical adsorption [26]. Besides, the Weber−Morris (W−M) intra-particle diffusion model [27], the Dumwald−Wagner (D−W) internal diffusion model [28], and the Boyd liquid film diffusion model [29] were adopted to ascertain the rate control step for vanadium adsorption. The W−M intra-particle diffusion model is based on the mass balance equation, which ignores the liquid film diffusion resistance of the adsorbent surface. The model hypothesizes that the diffusion of the ions inside the pores is the main factor that affects the adsorption rate [27]. The Boyd liquid film diffusion model assumes that adsorption resistance is concentrated at the boundary of the adsorbent particles [29].

The pseudo-first-order, pseudo-secondary-order kinetic, and Elovich kinetic models are presented as Eqs. (2)−(4) respectively [24]:

$$q_t = q_e(1 - \exp(-k_1 t)) \quad (2)$$

$$q_t = \frac{q_e^2 k_2 t}{1 + q_e k_2 t} \quad (3)$$

$$q_t = b\ln(ab) + \ln t \quad (4)$$

where q_t and q_e represent the amount of vanadium adsorbed at time t and at equilibrium, respectively (mg/g), k_1 is the

first-order adsorption rate constant (min^{-1}), k_2 is the second-order adsorption rate constant ($g \cdot mg^{-1} \cdot min^{-1}$), b is the desorption constant related to the surface coverage (g/mg), and a is the initial adsorption rate ($mg \cdot g^{-1} \cdot min^{-1}$).

The W−M intra-particle diffusion model is represented as [30]:

$$q_t = k_{ip} t^{\frac{1}{2}} + C \tag{5}$$

where C is related to the thickness of the boundary layer, and k_{ip} represents the intra-particle diffusion rate constant ($mg \cdot g^{-1} \cdot min^{-1}$).

The D−W internal diffusion equation is based on the following equation [28]:

$$F = 1 - \frac{6}{\pi^2} \sum_{n=1}^{\infty} \frac{1}{n^2} \exp(-n^2 \cdot B \cdot t) \tag{6}$$

The following equations were obtained through Fourier transform:

$$B \cdot t = \left(\pi^{1/2} - \sqrt{\pi - \frac{\pi^2 F}{3}} \right)^2, \ F < 0.85 \tag{7}$$

$$B \cdot t = -0.498 - \ln(1 - F), \ F > 0.85 \tag{8}$$

where F is the adsorption separation coefficient, $F = q_t/q_e$, and B and n are the empirical coefficients of D−W internal diffusion equation.

The Boyd liquid film diffusion model is given as follows [29]:

$$-\ln(1 - F) = k_{fd} \cdot t \tag{9}$$

where k_{fd} is the film diffusion mass transfer coefficient (min^{-1}).

2.6. Adsorption isotherm models

At a given temperature, the mass of an adsorbed solute at various concentrations is given by adsorption isotherm models [31]. Different adsorption isotherm models have been offered in this regard, and the most common and widely used models are Langmuir and Freundlich isotherm equations. The Langmuir isotherm model is based on the assumptions that the adsorption of ions on the adsorbent surface is a monolayer adsorption [32]. The Freundlich isotherm model assumes that the surface of the adsorbent is characterized by a distribution of adsorption sites that have different adsorption energies, and it describes the multilayer and reversible adsorption over a heterogeneous surface [33].

The linear expression of the Langmuir and Freundlich models are respectively given by the following equations [31]:

$$\frac{C_e}{q_e} = \frac{1}{Q_0} \cdot C_e + \frac{1}{K_L \cdot Q_0} \tag{10}$$

$$\ln q_e = \frac{1}{n} \cdot \ln C_e + \ln K_F \tag{11}$$

where C_e is the equilibrium concentrations of vanadium (mg/L), Q_0 depicts the maximum adsorption capacity (mg/g), K_L is the Langmuir adsorption constant (L/mg), K_F is the Freundlich adsorption constant, which represents the adsorption capacity (mg/g), and $1/n$ is the factor indicating how favorable the adsorption process is. $n > 1$ represents favorable adsorption condition.

3. Results and discussion

3.1. Electrode properties

3.1.1. S_{BET} and pore properties

The S_{BET} and pore properties of three D806/AC composite electrodes are presented in Table 1. The composite electrode with middle resin size poses higher S_{BET}, mesopore volume (V_{mes}), micropore volume (V_{mic}), and mesopore percentage (H_{mes}) than the other two electrodes, indicating that the appropriate resin size is conducive to the formation of a suitable pore structure and S_{BET} for the electrodes. If the resin particle size is extremely small, then the structure of the composite material may be damaged and can cause blockage of the pores, which is detrimental to the ions' transfer and adsorption. If the particle size is extremely large, then the composite electrode material has a small specific surface area. In addition, the material containing large particle resin is easily detached from the graphite during preparation and use, and the electrode surface is uneven. Thus, the resin particle size in the resin/activated carbon composite electrode should be moderate.

Table 1. S_{BET} and pore properties of different composite electrodes

Electrode	d / μm	S_{BET} / ($m^2 \cdot g^{-1}$)	V_{mic} / ($cm^3 \cdot g^{-1}$)	V_{mes} / ($cm^3 \cdot g^{-1}$)	H_{mes} / %
D860/AC C	125−150	493	0.259	0.132	33.76
D860/AC M	53−63	562	0.312	0.267	46.11
D860/AC S	37−45	529	0.279	0.144	34.04

Note: d is the particle size of resin.

3.1.2. FT-IR spectra

The FT-IR spectra of D860/AC M before and after vanadium adsorption are presented in Fig. 2. The peak at 3400 cm^{-1}, which is assigned to the stretching vibration of –OH [34], shifts to 3434 cm^{-1} after the adsorption. The adsorption peak observed at 2938 cm^{-1} corresponds to the C−H stretching vibration, which shifts to 2910 cm^{-1} after the adsorption. The adsorption peak observed at 1626 cm^{-1} is attributed to

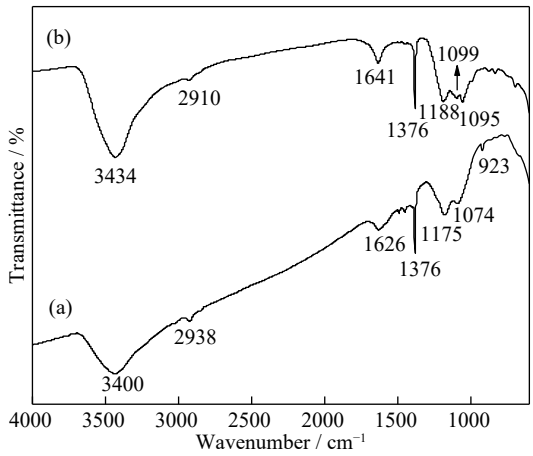

Fig. 2. FT-IR spectra of D860/AC M composite electrodes before (a) and after (b) adsorption.

the N−H stretching vibration, which shifts to 1641 cm^{-1} after the adsorption. The adsorption peak observed at 1175 cm^{-1} is attributed to the P=O stretching vibration, which also shifts to 1188 cm^{-1} after the adsorption. Furthermore, the peak near 1074 cm^{-1} is attributed to the N−C stretching vibration and PO_3^{2-} anti-symmetric stretching vibration, which moves to 1095 cm^{-1}. The adsorption peak at 923 cm^{-1} is specified to P−O−H functional group, which disappears after the adsorption. These changes indicate that the functional groups in D860 resin were modified after reacting with vanadium as shown in Eq. (12) [20].The new peak at 1099 cm^{-1} is caused by N−V coordination, which is associated with the migration of N−H and N−C characteristic peaks. In addition, the migration of P=O stretching vibration peak is also due to the chelation bonds between resin and vanadium (Eq. (12)).

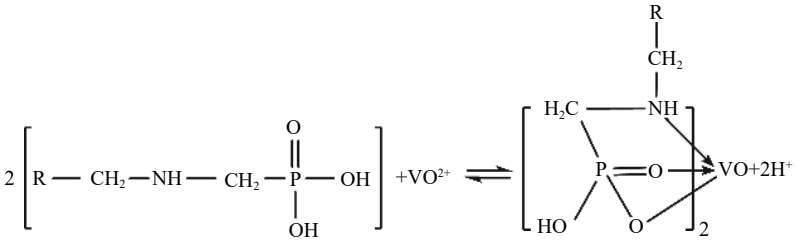

(12)

3.1.3. Electrochemical characteristics

The CV curves and Nyquist plot of three composite electrodes are shown in Figs. 3 and 4, respectively. The area enclosed by the CV curve represents the specific capacitance of the electrodes. The specific capacitances of different electrodes follow the ascending order: D860/AC C (15.24 F/g) < D860/AC S (24.76 F/g) < D860/AC M (39.66 F/g), which is the same as the order of S_{BET} and H_{mes} (Table 1). The result indicates that the specific capacitance of the composite electrode strongly depends on S_{BET} and H_{mes}, and the electrode with larger S_{BET} can provide more active sites for ions adsorption [35].

The Nyquist plot consists of a nearly vertical line in the low-frequency region and a semi-circle in the high-frequency region. The vertical line corresponds to the ion diffusion inside the electrode, and the semi-circle is related to charge transfer resistance on the interface between the electrode and electrolyte [36−37]. A large semi-circle diameter means a large contact resistance and a steep vertical line indicates a small impedance for ions. Fig. 4 shows that D860/AC M has the smallest diameter of the semi-circle in the high-frequency region and the largest slope in the low-frequency region, demonstrating that D860/AC M has the highest electric conductivity and lowest internal resistance, which is conducive to ion adsorption on the electrode.

The alternating current impedance curve was fitted by

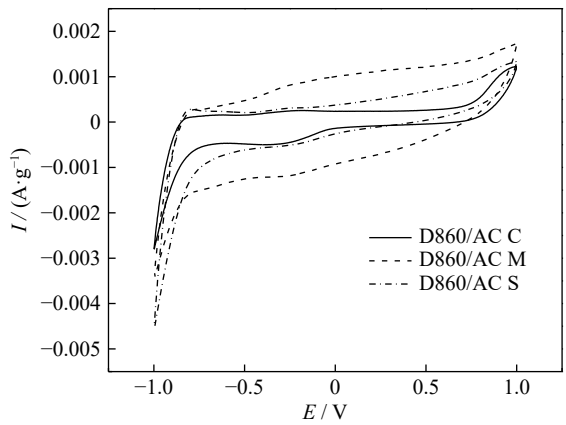

Fig. 3. CV curves of different composite electrodes.

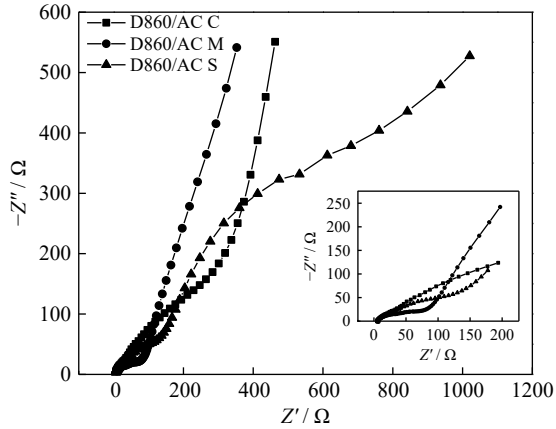

Fig. 4. Nyquist plot of different composite electrodes.

ZSimpWin software. The results including those for the equivalent circuit are illustrated in Fig. 5. The adsorption dynamic parameters of ions on the electrodes are presented in Table 2, where R_s represents the solution resistance and R_{ct} stands for the electron transfer resistance. The current flowed through the solution and interface in turn, so R_s and R_{ct} belong to the series relationship. C_{dl} is the EDL capacitor. As the interface electronic transfer voltage is determined by the charge of the EDL, so R_{ct} and C_{dl} are in a parallel relationship. W is the Warburg impedance, which is linked to the concentration difference caused by diffusion and IX reaction. R_1 represents the impedance of internal diffusion. The IX reaction occurs at the same time as internal diffusion. Thus, W and R_1 have the same chemical rate, which can be attributed to the series relationship in the circuit. CPE is a constant phase angle element, which is related to surface adsorption (Fig. 5(b)). When the ions are adsorbed on the electrode surface, the surface non-uniformity of the electrode cannot be ignored; thus, the CPE is introduced in the circuit. It can be found from Fig. 5 that the experimental data are consistent with the fitting values, thereby verifying the reliability of the equivalent circuit.

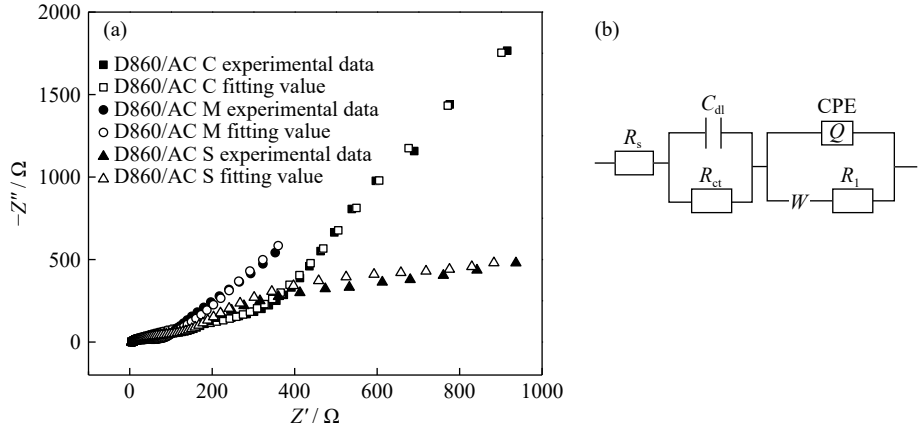

Fig. 5. Equivalent circuit diagram of circuit fitting curve (a) and equivalent circuit (b).

Table 2. Parameters of equivalent circuits

Electrode	R_s / Ω	C_{dl} / F	R_{ct} / Ω	W	R_1 / Ω
D860/AC C	4.221	0.0058	769.7	0.0046	362.8
D860/AC M	5.449	0.0471	624.8	0.0099	60.42
D860/AC S	4.814	0.0096	391.0	0.0672	148.9

Table 2 shows that R_s of the three composite electrodes does not change significantly. It is only related to experimental conditions such as temperature and ion concentration. R_{ct} increases with the increase of resin size in the composite electrode, indicating that the electrode made of coarser resin has higher electrode conductivity. The surface of the electrodes may be occupied by more resins as the resin size increases, thereby resulting in the increase of R_{ct} because the resin is non-conducting. C_{dl} is consistent with the specific capacitance measured by CV. The R_1 values of different electrodes follow the ascending order: D860/AC M < D860/AC S < D860/AC C, which is negatively correlated with the H_{mes} of the electrodes. The increase in the diffusion path generally leads to an increase in R_1. Thus, we can infer that the mesoporous may facilitate ion diffusion within the composite electrode. The R_1 of D860/AC M is the smallest, so the diffusion path is the shortest, which shows that this composite electrode may be suitable for ion adsorption in CDI.

3.2. Effect on adsorption capacity of V(IV)

The adsorption capacity for V(IV) calculated according to Eq. (1) at different times is shown in Fig. 6. The equilibrium adsorption capacities of different electrodes for V(IV) follow the order: D860/AC C < D860/AC S < D860/AC M. The composite electrode with more mesoporous percentage has a larger equilibrium adsorption capacity. We find evidence that the electro-sorption capacity has a close relation with the V_{mes} of the electrode materials, and V(IV) is mainly adsorbed in

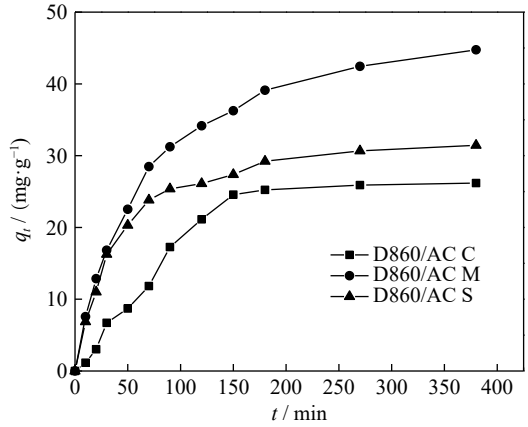

Fig. 6. Adsorption curves of composite electrodes with different resin particle sizes.

the mesoporous content of the composite electrode [38].

3.3. Adsorption kinetics

The electrode adsorption process includes three consecutive steps in general. The ions in the aqueous solution migrate through the liquid film to the electrode surface (liquid film diffusion). The ions diffuse from the electrode surface to the internal pores of the electrode (intra-particle diffusion). Finally, the ions are adsorbed at active sites on the pore wall (adsorption reaction). Commonly, the last step is fast and negligible, so the adsorption rate is controlled by one of the former two or perhaps both steps. The adsorption of V(IV) on the electrodes can be divided into two stages, i.e., the first fast adsorption stage (stage I) and the second gradual adsorption stage (stage II) (Fig. 7). Stages I and II were fitted with the W−M intra-particle diffusion and Boyd liquid film diffusion models, respectively (Fig. 7). The fitting parameters are shown in Table 3.

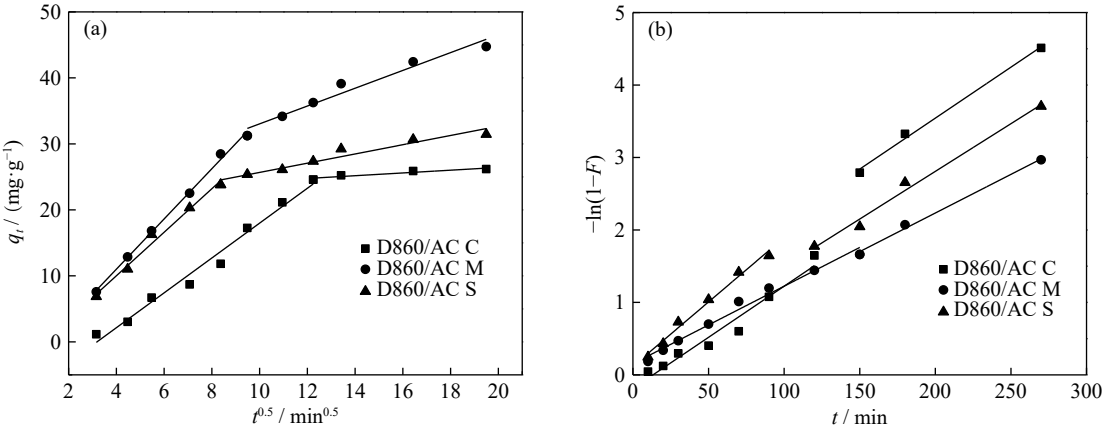

Fig. 7. Adsorption fitting of V(IV) using W−M intra-particle (a) and Boyd liquid film (b) diffusion models.

Table 3. Fitting parameters of V(IV) adsorption in different models

Adsorption kinetics model		W−M intra-particle diffusion		Boyd liquid film diffusion	
		k_{ip} / (mg·g^{-1}·min^{-1})	R^2	k_{fd} / min^{-1}	R^2
D860/AC C	Stage I	2.6415	0.9791	0.0182	0.9164
	Stage II	0.2090	0.8499	0.0141	0.9912
D860/AC M	Stage I	3.9540	0.9981	0.0107	0.9801
	Stage II	1.4654	0.9497	0.0107	0.9902
D860/AC S	Stage I	3.2987	0.9805	0.0178	0.9839
	Stage II	0.6994	0.9266	0.0132	0.9836

Note: k_{ip} and k_{fd} are adsorption rate constants; R^2 is goodness of fit.

The fitting lines in Fig. 7 do not go through the origin, indicating that the adsorption rate was not controlled by sole step [39−40]. The kinetic fitting parameters in Table 3 show that the intra-particle diffusion model fits well at stage I while the liquid film diffusion model presents good R^2 at stage II. We can conclude that at stage I, the ions passed through the liquid film to reach the electrode surface under the combination of electrostatic attraction and electric field force. Then, the intra-particle diffusion occurred leading to a slow diffusion rate in the internal particles due to the pore resistance. D860/AC M had the largest intra-particle diffusion constant, which was consistent with the impedance of internal diffusion (Table 2). The D−W internal diffusion model was used to fit the adsorption process of the ions at stage I, and R^2 is greater than 0.99 (Fig. 8), which verified the conclusion that the intra-particle diffusion is the rate-controlling step at stage I.

During the adsorption process, the EDL charge gradually increased and the charge on the electrode surface was offset.

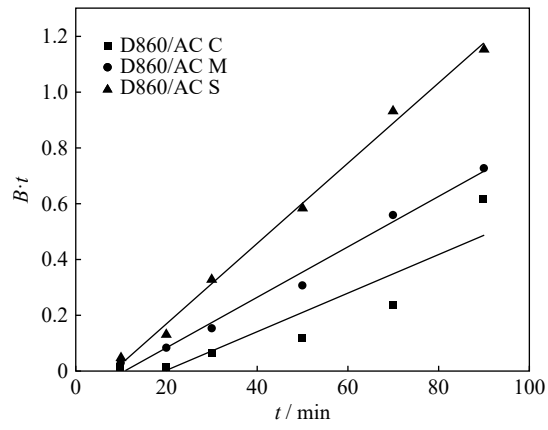

Fig. 8. Adsorption fitting of V(IV) using D−W diffusion model.

Thus, the electrostatic attractive force was gradually reduced and the driving force for the liquid film diffusion was gradually reduced to make the liquid film diffusion rate smaller than the intra-particle diffusion rate. Thus, the liquid film diffusion is the rate-controlling step at stage II. Table 3 shows that the composite electrode with more abundant mesoporous content has the larger adsorption rate constant, indicating that the ions diffuse more easily in mesopores, which is in accordance with the results of EIS and the equivalent circuit analysis.

The adsorption processes of V(IV) on the composite electrodes were also fitted by the pseudo-first-order and pseudo-second-order kinetic models. The results are presented in Fig. 9 and Table 4.

We found that both the pseudo-second-order and pseudo-first-order kinetic models could successfully depict the adsorption process at stage I. R^2 was above 0.99, indicating that the chemical adsorption and physical adsorption occurred simultaneously during the adsorption of V(IV) on the composite electrodes. Nevertheless, the R^2 of the pseudo-second-order kinetic model (0.988−0.999) was higher than that of the pseudo-first-order kinetic model (0.958−0.966) at stage II.

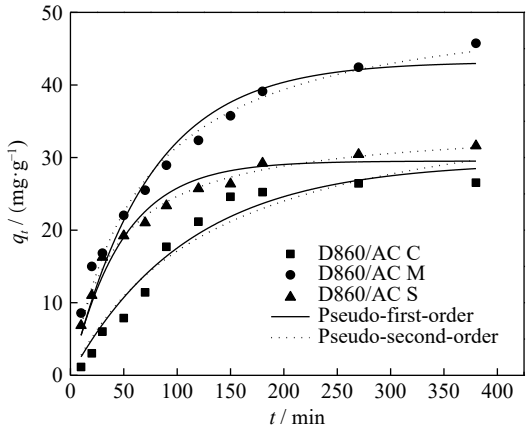

Fig. 9. Adsorption kinetic curves obtained from two kinetic models.

During the adsorption process, V(IV) was stored first in the EDL and then exchanged with the resins [21]. The IX reactions were characterized as chemical and were more complex and slower than the electrostatic attraction. Thus, at stage II, the adsorption of V(IV) was mainly controlled by chemisorption.

Table 4. Kinetic parameters of V(IV) adsorption on composite electrodes

Adsorption kinetics model		Pseudo-first-order				Pseudo-first-order		
		k_1 / min^{-1}	R^2	$q_{e,exp}$ / (mg·g^{-1})	$q_{e,cal}$ / (mg·g^{-1})	k_2 / (g·mg^{-1}·min^{-1})	R^2	$q_{e,cal}$ / (mg·g^{-1})
D860/AC C	Stage I	0.0046	0.988	26.70	29.30	0.0002	0.987	34.74
	Stage II	0.0186	0.9576			0.0028	0.988	
D860/AC M	Stage I	0.0176	0.9937	45.63	43.20	0.0003	0.9976	52.50
	Stage II	0.011	0.9663			0.0003	0.9997	
D860/AC S	Stage I	0.0262	0.9910	31.75	29.52	0.0007	0.9895	40.13
	Stage II	0.0146	0.9644			0.0011	0.997	

Note: k_1 and k_2 are adsorption rate constants; $q_{e,exp}$ is the experimental adsorption capacity; $q_{e,cal}$ is the calculated adsorption capacity.

The Elovich kinetic equation was primarily used to characterize the chemical adsorption process of gas on the solid surface [41], and it was used in the present study to investigate the adsorption of V(IV) in CDI. Table 5 shows that this model does not fit the adsorption well for the D860/AC C and D860/AC S electrodes, implying that the adsorption process of V(IV) on the composite electrodes is different from the gas adsorption. The ion adsorption was affected by the intermolecular action and relative molecular mass, and the ions should pass through the liquid film to be adsorbed [42]. This process was relatively slow and different from the gas adsorption. Thus, the adsorption of V(IV) on D860/AC C and D860/AC S did not fit the Elovich kinetic equation. However, the EIS analysis indicated that D860/AC M had small R (Table 2) and ions had better diffusion performance on it than the two electrodes. Thus, the Elovich kinetic equation fit the adsorption of V(IV) on D860/AC M better than that on D860/AC C and D860/AC S.

Table 5. Elovich model parameters for V(IV) adsorption on electrodes

Kinetics model	Electrode	R^2	a / (mg·g^{-1}·min^{-1})	b / (g·mg^{-1})
Elovich model	D860/AC C	0.9305	0.6971	0.1199
	D860/AC M	0.9911	1.9406	0.0912
	D860/AC S	0.9662	2.1805	0.1403

3.4. Adsorption isotherms

Fig. 10 shows the linear fitting of the Langmuir and Freundlich models for the experimental results and the fitting parameters are shown in Table 6. The isotherm plots (Fig. 10) and derived parameters (Table 6) show that the adsorption of vanadium on the composite electrode is more fitted to the Freundlich model (R^2 = 0.998) than the Langmuir model (R^2 = 0.975), suggesting that V(IV) is adsorbed heterogeneously onto the composite electrode as multilayers [33]. In addition, the Freundlich model indicates that the adsorption

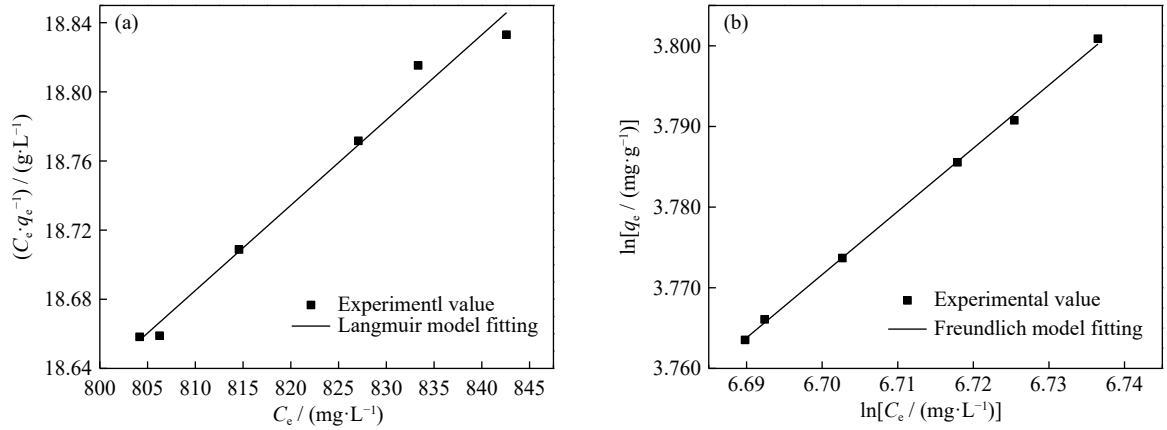

Fig. 10. Linear fitting curves of Langmuir (a) and Freundlich (b) isotherm models of V(IV) adsorption on D860/AC M.

Table 6. Isotherm model constants for V(IV) adsorption on D860/AC M

Langmuir constants			Freundlich constants		
K_L / (L·mg^{-1})	Q_0 / (mg·g^{-1})	R^2	K_F / (mg·g^{-1})	1/n	R^2
0.0004	185.19	0.975	0.23	0.78	0.998

sites for V(IV) are not unique, indicating that V(IV) not only is adsorbed on the AC to form EDL, but also interacts with resins, as validated by the kinetic study. Moreover, the value of the Freundlich constant (1/n = 0.78) proved that V(IV) is easily adsorbed by D860/AC M.

3.5. Adsorption thermodynamics

Based on the van't Hoff equation, the enthalpy change (ΔH) and entropy change (ΔS) of the adsorption process can be calculated as [43]

$$\ln k_d = -\frac{\Delta H}{RT} + \frac{\Delta S}{R} \tag{13}$$

where R = 8.314 J/(mol·K), k_d is the thermodynamic equilibrium constant, and T is the absolute temperature (K). The ΔS and ΔH can be calculated from the intercept and slope of the fitting line. The equation was used to fit the adsorption experimental data as shown in Fig. 11.

The Gibbs free energy was obtained by the following equations [44]:

$$\Delta G = -RT\ln k_d \tag{14}$$

$$\Delta G = \Delta H - T \cdot \Delta S \tag{15}$$

Thus, the adsorption thermodynamic parameters of V(IV) on D860/AC M can be obtained as shown in Table 7.

Table 7 shows that ΔH is negative, indicating that the adsorption of V(IV) in CDI is an exothermic process, thereby raising the temperature is not conducive to the ions adsorption on the composite electrodes. In addition, the decrease of entropy with the adsorption ($\Delta S < 0$) means that the system disorder degree was reduced as free moving vanadium ions in the aqueous solution were adsorbed on the electrodes [45]. $\Delta G > 0$ indicates that the chemical potential was elevated with the adsorption. Besides the change in chemical potential, an electric field force also had a nonvolumetric function in the CDI process. Therefore, ΔG cannot be used to judge the direction of the adsorption in CDI. If the decrease of the electric potential energy is more than the increase of chemical potential energy, then the change of the total energy of the CDI system is less than 0 and the adsorption process can proceed. The ions move under the action of an electric field force, which leads to the reduction of electric potential en-

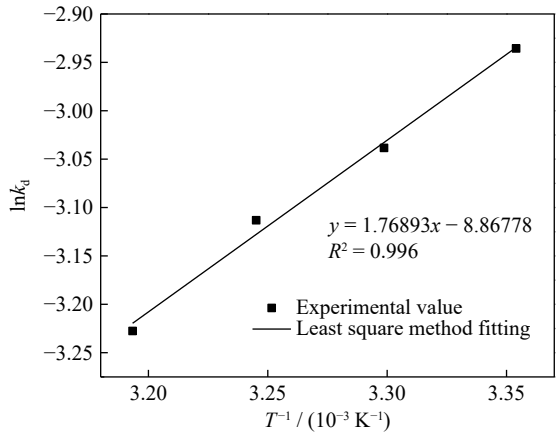

Fig. 11. Fitting curve of van't Hoff equation of V(IV) adsorption on D860/AC M.

Table 7. Thermodynamic parameters of V(IV) adsorption on D860/AC M

T / K	ΔG / (kJ·mol^{-1})	ΔH / (kJ·mol^{-1})	ΔS / (J·mol^{-1}·K^{-1})
298	7.27	−14.71	−73.73
303	7.64		
308	8.01		
313	8.38		

ergy. The reduced potential energy is converted into kinetic energy for ion migration and chemical potential energy for IX reaction, which shows that the electric field force plays a dominant role in the CDI process.

4. Conclusions

(1) The appropriate resin size was conducive to the formation of a suitable pore structure for the composite electrodes. The composite electrode made of middle resin size (D860/AC M) had the largest specific surface area and mesoporous content than the other two composite electrodes. Electrochemical analysis results also showed that D860/AC M exhibited higher specific capacitance and EDL capacitor, and significantly lower impedance of internal diffusion, thereby causing the D860/AC M to present the highest adsorption capacity and fastest adsorption rate for V(IV) in CDI.

(2) The adsorption process of V(IV) on the composite electrodes in CDI can be divided into two stages. The ion adsorption on the composite electrodes was controlled by intraparticle diffusion in the initial stage and the liquid film diffusion determined the adsorption in the second stage.

(3) During the V(IV) adsorption process, the vanadium ions were first adsorbed on the EDL and then exchanged with the resin in the composite electrode. Physisorption and chemisorption occurred simultaneously in the entire process. Moreover, the adsorption isotherms indicated that V(IV) was adsorbed heterogeneously on the composite electrode as multilayers in CDI.

(4) The adsorption of V(IV) on the composite electrode in CDI was an exothermic process with entropy reduction. Moreover, the adsorption of ions in CDI was strongly dependent on the electric field.

Acknowledgement

This work was financially supported by the National Natural Science Foundation of China (No. 51874222).

References

[1] M.T. Li, C. Wei, G. Fan, H.L. Wu, C.X. Li, and X.B. Li, Acid leaching of black shale for the extraction of vanadium, *Int. J. Miner. Process.*, 95(2010), No. 1-4, p. 62.

[2] Y.M. Zhang, S.X. Bao, T. Liu, T.J. Chen, and J. Huang, The technology of extracting vanadium from stone coal in China: History, current status and future prospects, *Hydrometallurgy*, 109(2011), No. 1-2, p. 116.

[3] B. Chen, S.X. Bao, Y.M. Zhang, and S. Li, A high-efficiency and sustainable leaching process of vanadium from shale in sulfuric acid systems enhanced by ultrasound, *Sep. Purif. Technol.*, 240(2020), art. No. 116624.

[4] B. Chen, S.X. Bao, and Y.M. Zhang, Column separation of vanadium(v) from complex sulfuric solution using trialkylamine-impregnated resins, *JOM*, 72(2020), No. 2, p. 953.

[5] R. Navarro, J. Guzman, I. Saucedo, J. Revilla, and E. Guibal, Vanadium recovery from oil fly ash by leaching, precipitation and solvent extraction processes, *Waste Manag.*, 27(2006), No. 3, p. 425.

[6] Y.P. Luo, S.X. Bao, and Y.M. Zhang, Preparation of one-part geopolymeric precursors using vanadium tailing by thermal activation, *J. Am. Ceramic. Soc.*, 103(2020), No. 2, p. 779.

[7] B. Chen, S.X. Bao, and Y.M. Zhang, Synergetic strengthening mechanism of ultrasound combined with calcium fluoride towards vanadium extraction from low-grade vanadium-bearing shale, *Int. J. Min. Sci. Technol.* (2021). DOI: 10.1016/j.ijmst.2021.07.008

[8] W. Li, Y.M. Zhang, T. Liu, J. Huang, and Y. Wang, Effect of impurities on vanadium purification from acid leaching solution of stone coal with solvent extraction process, *Nonferrous Met. Extr. Metall.*, 2013, No. 5, p. 27.

[9] L. Liang, S.X. Bao, Y.M. Zhang, and Y.P. Tang, Separation and recovery of V(IV) from sulfuric acid solutions containing Fe(III) and Al(III) using bis(2-ethylhexyl)phosphoric acid impregnated resin, *Chem. Eng. Res. Des.*, 111(2016), p. 109.

[10] Y.P. Tang, S.X. Bao, Y.M. Zhang, and L. Liang, Effect of support properties on preparation process and adsorption performances of solvent impregnated resins, *React. Funct. Polym.*, 113(2017), p. 50.

[11] Z.H. Huang, Z.Y. Yang, F.Y. Kang, and M. Inagaki, Carbon electrodes for capacitive deionization, *J. Mater. Chem. A*, 5(2017), No. 2, p. 470.

[12] C.Y. Zhang, D. He, J.X. Ma, W.W. Tang, and T.D. Waite, Faradaic reactions in capacitive deionization (CDI) - problems and possibilities: A review, *Water Res.*, 128(2018), p. 314.

[13] Y. Oren, Capacitive deionization (CDI) for desalination and water treatment — Past, present and future (a review), *Desalination*, 228(2008), No. 1-3, p. 10.

[14] K.B. Hatzell, E. Iwama, A. Ferrs, B. Daffos, K. Urita, T. Tzedakis, F. Chauvet, P.L. Taberna, Y. Gogotsi, and P. Simon, Capacitive deionization concept based on suspension electrodes without ion exchange membranes, *Electrochem. Commun.*, 43(2014), p. 18.

[15] J.Y. Zhou, Y.M. Zhang, and S.X. Bao, Preparation and selective adsorption property of the ion-exchange resin/carbon composite electrode, *Ind. Saf. Environ. Prot.*, 42(2016), No. 12, p. 51.

[16] Y.J. Kim and J.H. Choi, Selective removal of nitrate ion using a novel composite carbon electrode in capacitive deionization, *Water Res.*, 46(2012), No. 18, p. 6033.

[17] D.H. Lee, T. Ryu, J. Shin, J.C. Ryu, K.S. Chung, and Y.H. Kim, Selective lithium recovery from aqueous solution using a modified membrane capacitive deionization system, *Hydrometallurgy*, 173(2017), p. 283.

[18] J.H. Yeo and J.H. Choi, Enhancement of nitrate removal from a solution of mixed nitrate, chloride and sulfate ions using a nitrate-selective carbon electrode, *Desalination*, 320(2013), p. 10.

[19] Y.Y. Cui, S.X. Bao, Y.M. Zhang, and J.H. Duan, Adsorption characteristics of vanadium on different resin-active carbon composite electrodes in capacitive deionization, *Chemosphere*, 212(2018), p. 34.

[20] J.H. Duan, S.X. Bao, and Y.M. Zhang, The characteristics of resin/carbon composite electrode and application in selective adsorption of vanadium(IV) by capacitive deionization, *Chem. Eng. Res. Des.*, 132(2018), p. 178.

[21] S.X. Bao, J.H. Duan, and Y.M. Zhang, Recovery of V(V) from complex vanadium solution using capacitive deionization (CDI)

with resin/carbon composite electrode, *Chemosphere*, 208(2018), p. 14.
[22] J. Villarroel-Rocha, D. Barera, and K. Sapag, Introducing a self-consistent test and the corresponding modification in the Barrett, Joyner and Halenda method for pore-size determination, *Microporous Mesoporous Mater.*, 200(2014), p. 68.
[23] H. Yuh-shan, Citation review of Lagergren kinetic rate equation on adsorption reactions, *Scientometrics*, 59(2004), No. 1, p. 171.
[24] P.J. Lin, J.J. Wu, J.M. Ahn, and J. Lee, Adsorption characteristics of Cd(II) and Ni(II) from aqueous solution using succinylated hay, *Int. J. Miner. Metall. Mater.*, 26(2019), No. 10, p. 1239.
[25] N. Öztürk and T.E. Köse, A kinetic study of nitrite adsorption onto sepiolite and powdered activated carbon, *Desalination*, 223(2008), No. 1-3, p. 174.
[26] Y.S. Ho and G. Mckay, A comparison of chemisorption kinetic models applied to pollutant removal on various sorbents, *Process Saf. Environ. Prot.*, 76(1998), No. 4, p. 332.
[27] A. Sari, M. Tuzen, D. Citak, and M. Soylak, Equilibrium, kinetic and thermodynamic studies of adsorption of Pb(II) from aqueous solution onto Turkish kaolinite clay, *J. Hazard. Mater.*, 149(2007), No. 2, p. 283.
[28] G.E. Boyd, A.W. Adamson, and L.S. Myers, The exchange adsorption of ions from aqueous solutions by organic zeolites: Kinetics, *J. Am. Chem. Soc.*, 69(1947), No. 11, p. 2836.
[29] M.K. Aroua, S.P.P. Leong, L.Y. Teo, C.Y. Yin, and W.M.A.W. Wandaud, Real-time determination of kinetics of adsorption of lead(II) onto palm shell-based activated carbon using ion selective electrode, *Bioresour. Technol.*, 99(2008), No. 13, p. 5786.
[30] D.E. Egirani, N.R. Poyi, and N. Wessey, Synthesis of a copper(II) oxide–montmorillonite composite for lead removal, *Int. J. Miner. Metall. Mater.*, 26(2019), No. 7, p. 803.
[31] E.Z. Li, H.B. Liang, Z.P. Du, D. Li, and F.Q. Cheng, Adsorption process of Octadecylamine Hydrochloride on KCl crystal surface in various salt saturated solutions: Kinetics, isotherm model and thermodynamics properties, *J. Mol. Liq.*, 221(2016), p. 949.
[32] Y.X. He, L.M. Zhang, X. An, G.P. Wan, W.J. Zhu, and Y.M. Luo, Enhanced fluoride removal from water by rare earth (La and Ce) modified alumina: Adsorption isotherms, kinetics, thermodynamics and mechanism, *Sci. Total Environ.*, 688(2019), p. 184.
[33] Y. Wimalasiri, M. Mossad, and L.D. Zou, Thermodynamics and kinetics of adsorption of ammonium ions by graphene laminate electrodes in capacitive deionization, *Desalination*, 357(2015), p. 178.
[34] X.C. Lu, J.C. Jiang, K. Sun, X.P. Xie, and Y.M. Hu, Surface modification, characterization and adsorptive properties of a coconut activated carbon, *Appl. Surf. Sci.*, 258(2012), No. 20, p. 8247.
[35] W.L. Zhang, J. Yin, Z.Q. Lin, H.B. Lin, H.Y. Lu, Y. Wang, and W.M. Huang, Facile preparation of 3D hierarchical porous carbon from lignin for the anode material in lithium ion battery with high rate performance, *Electrochim. Acta*, 176(2015), p. 1136.
[36] J.Y. Liu, S.P. Wang, J.M. Yang, J.J. Liao, M. Lu, H.J. Pan, and L. An, $ZnCl_2$ activated electrospun carbon nanofiber for capacitive desalination, *Desalination*, 344(2014), p. 446.
[37] X. Liu, T. Chen, W.C. Qiao, Z. Wang, and L. Yu, Fabrication of graphene/activated carbon nanofiber composites for high performance capacitive deionization, *J. Taiwan Inst. Chem. Eng.*, 72(2017), p. 213.
[38] P.I. Liu, L.C. Chung, C.H. Ho, H. Shao, T.M. Liang, M.C. Chang, C.C.M. Ma, and R.Y. Horng, Comparative insight into the capacitive deionization behavior of the activated carbon electrodes by two electrochemical techniques, *Desalination*, 379(2016), p. 34.
[39] Y. Li, Q. Xie, W. Yan, Y. Wang, and Z.H. Zhang, Adsorption of K^+ from an aqueous phase onto an activated carbon used as an electric double-layer capacitor electrode, *Min. Sci. Technol. China*, 20(2010), No. 4, p. 551.
[40] K. Navneet, K. Manpreet, and S. Dhanwinder, Fabrication of mesoporous nanocomposite of graphene oxide with magnesium ferrite for efficient sequestration of Ni(II) and Pb(II) ions: Adsorption, thermodynamic and kinetic studies, *Environ. Pollut.*, 253(2019), p. 111.
[41] C. Aharoni and F.C. Tompkins, Kinetics of adsorption and desorption and the Elovich equation, *Adv. Catal.*, 21(1970), p. 1.
[42] Y.Y. Liu, Y. Xiong, P. Xu, Y. Pang, and C.Y. Du, Enhancement of Pb(II) adsorption by boron doped ordered mesoporous carbon: Isotherm and kinetics modeling, *Sci. Total Environ.*, 708(2020), No. 15, art. No. 134918.
[43] N. Boukhalfa, M. Boutahala, N. Djebri, and A. Idris, Kinetics, thermodynamics, equilibrium isotherms, and reusability studies of cationic dye adsorption by magnetic alginate/oxidized multiwalled carbon nanotubes composites, *Int. J. Biol. Macromol.*, 123(2019), p. 539.
[44] Q. Tian, J.G. Yang, and X.J. Bai, Insight into the change in carbon structure and thermodynamics during anthracite transformation into graphite, *Int. J. Miner. Metall. Mater.*, 27(2020), No. 2, p. 162.
[45] Q.L. Hong, Y.H. Dong, W. Zuang, C. Rao, and C. Liu, Kinetics and thermodynamics of lysozyme adsorption on mesoporous titanium dioxide, *Acta Phys. Chim. Sin.*, 32(2016), No. 3, p. 638.